

Local Spin Anisotropy Effects upon the Magnetization of Single Molecule Dimers

Dmitri V. Efremov^{1,*} and Richard A. Klemm^{2,†}

¹*Institut für Theoretische Physik, Technische Universität Dresden, 01062 Dresden, Germany*

²*Department of Physics, Kansas State University, Manhattan, KS 66506 USA*

(Dated: December 2, 2024)

We present an exactly solvable model of equal spin s_1 single molecule magnetic dimers. The spins within each dimer interact via the Heisenberg and the most general quadratic global and local anisotropic spin exchange interactions, and with the magnetic induction \mathbf{B} . For antiferromagnetic couplings and $s_1 > 1/2$, the low temperature magnetization $\mathbf{M}(\mathbf{B})$ exhibits a rich variety of steps of unequal width, the structure and anisotropy of which depend upon the various local anisotropic spin exchange energies. Our results are compared to experiments on Fe_2 dimers.

PACS numbers: 05.20.-y, 75.10.Hk, 75.75.+a, 05.45.-a

Single molecule magnets (SMM's) have been under intense study recently, due to their potential uses in magnetic storage and quantum computing.[1, 2, 3] The materials consist of insulating crystalline arrays of identical SMM's 1-3 nm in size, each containing two or more magnetic ions. Since the magnetic ions in each SMM are surrounded by non-magnetic ligands, the intermolecular magnetic interactions are usually negligible. Although the most commonly studied SMM's are the high-spin Mn_{12} and Fe_8 ,[1, 2, 3, 4, 5] such SMM's contain a variety of ferromagnetic (FM) and antiferromagnetic (AFM) intramolecular interactions, rendering unique fits to a variety of experiments difficult.[6]

In addition, there have been many studies of AFM Fe_n ring compounds, with $n = 6, 8, 10, 12$, etc.[7, 8, 9, 10] In these studies, analyses of inelastic neutron diffraction data and the magnetic induction \mathbf{B} dependence of the low-temperature T specific heat and magnetization steps were made, using the isotropic Heisenberg near-neighbor exchange interaction, the Zeeman interaction, and various near-neighbor spin anisotropy interactions.[7, 8, 9, 10] However, the rings were so complicated that analyses of the data using those simple models were inaccessible to present day computers.[8, 9] Thus, those authors used either simulations or phenomenological fits to a first-order perturbation expansion with different spin anisotropy values for each global ring spin value.[8, 9, 10]

Here we focus on the simpler cases of equal spin $s_1 = s_2$ magnetic dimers, for which the full spin anisotropy effects can be evaluated analytically, investigated in detail numerically, and compared with experiment. AFM dimers with $s_1 = 1/2, 3/2$,[11] and various forms of Fe_2 with $s_1 = 5/2$ were studied recently.[12, 13, 14, 15, 16, 17] Several Fe_2 dimers and effective $s_1 = 9/2$ dimers of the type $[\text{Mn}_4]_2$,[18, 19] have magnetic interactions weak enough that their effects can be probed at $T \approx 1\text{K}$ with presently available \mathbf{B} . A comparison of our calculated results with magnetization step data on Fe_2 dimers strongly suggests a substantial presence of local spin anisotropy.[14]

We represent the $s_1 = s_2$ dimer quantum states, $|\psi_s^m\rangle$ in terms of the global (total) spin and magnetic quantum

numbers s and m , where $\mathbf{S} = \mathbf{S}_1 + \mathbf{S}_2$ and $S_z = \mathbf{S} \cdot \hat{\mathbf{z}}$ satisfy $\mathbf{S}^2|\psi_s^m\rangle = s(s+1)|\psi_s^m\rangle$ and $S_z|\psi_s^m\rangle = m|\psi_s^m\rangle$, where $s = 0, 1, \dots, 2s_1$, $m = -s, \dots, s$, and we set $\hbar = 1$. We also have $S_{\pm}|\psi_s^m\rangle = A_s^{\pm m}|\psi_s^{m\pm 1}\rangle$, where $S_{\pm} = S_x \pm iS_y$ and $A_s^m = \sqrt{(s-m)(s+m+1)}$. For an arbitrary \mathbf{B} , we assume the Hamiltonian has the form $\mathcal{H} = \mathcal{H}_0 + \mathcal{H}_a + \mathcal{H}_b + \mathcal{H}_c + \mathcal{H}_d$, where $\mathcal{H}_0 = -J\mathbf{S}^2/2 - g\mu_B\mathbf{S} \cdot \mathbf{B}$ contains the Heisenberg exchange and Zeeman interactions, $g \approx 2$ and μ_B is the Bohr magneton. The global anisotropy terms $\mathcal{H}_b = -J_bS_z^2$ and $\mathcal{H}_d = -J_d(S_x^2 - S_y^2)$ only involve components of \mathbf{S} , but have been the main anisotropy terms discussed in the SMM literature,[5, 18] so we have included them for comparison. The previously neglected local axial and azimuthal anisotropy terms,

$$\mathcal{H}_a = -J_a \sum_{i=1}^2 S_{iz}^2, \quad (1)$$

$$\mathcal{H}_c = -J_c(S_{1x}S_{2x} - S_{1y}S_{2y}), \quad (2)$$

arise from spin-orbit interactions of the local crystal field with the individual spins. Since $\sum_{i=1}^2 (S_{ix}^2 - S_{iy}^2) = 2\mathcal{H}_c/J_c - \mathcal{H}_d/J_d$, it is included. For the case of Fe_2 ,[12] a constituent of the high-spin SMM Fe_8 and the AFM Fe_n rings,[4, 8, 9] the exchange between the Fe^{+3} $s_1 = 5/2$ spins occurs via two oxygen ions, and these four ions essentially lie in the same (xz) plane.[12, 15] We set the z axis parallel to the dimer axis, as pictured in Fig. 1.

For $\mathbf{B} = B(\sin \theta \cos \phi, \sin \theta \sin \phi, \cos \theta)$, we have

$$\mathcal{H}_0|\psi_s^m\rangle = E_s^m|\psi_s^m\rangle + \delta E \sum_{\sigma=\pm 1} e^{-i\sigma\phi} A_s^{\sigma m}|\psi_s^{m+\sigma}\rangle, \quad (3)$$

$\mathcal{H}_d|\psi_s^m\rangle = \frac{-J_d}{2} \sum_{\sigma=\pm 1} F_s^{\sigma m}|\psi_s^{m+2\sigma}\rangle$, and $\mathcal{H}_b|\psi_s^m\rangle = -J_b m^2 |\psi_s^m\rangle$, where $E_s^m = -Js(s+1)/2 - mg\mu_B B \cos \theta$, $\delta E = -\frac{1}{2}g\mu_B B \sin \theta$, and $F_s^x = A_s^x A_s^{1+x}$. \mathcal{H}_a and \mathcal{H}_c contain the individual spin operators S_{iz} and $S_{i\pm}$ for $i = 1, 2$. After some Clebsch-Gordon algebra involving the Wigner-Eckart theorem, for arbitrary (s_1, s, m) ,

$$S_{i\pm}|\psi_s^m\rangle = \frac{1}{2} A_s^{\pm m}|\psi_s^{m\pm 1}\rangle - \frac{1}{2} (-1)^i (C_{s,s_1}^{\pm m}|\psi_{s-1}^{m\pm 1}\rangle$$

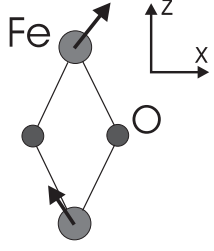


FIG. 1: Sketch of an Fe_2 dimer, with two bridging O^{-2} ions (O). Ligands (not pictured) are attached to the Fe^{+3} ions (Fe). The arrows signify spins.

$$-C_{s+1,s_1}^{-1\mp m}|\psi_{s+1}^{m\pm 1}\rangle), \quad (4)$$

$$S_{iz}|\psi_s^m\rangle = \frac{m}{2}|\psi_s^m\rangle - \frac{1}{2}(-1)^i\left(D_{s,s_1}^m|\psi_{s-1}^m\rangle + D_{s+1,s_1}^m|\psi_{s+1}^m\rangle\right), \quad (5)$$

where $C_{s,s_1}^m = \sqrt{(s-m)(s-m-1)}\eta_{s,s_1}$, $D_{s,s_1}^m = \sqrt{(s^2-m^2)}\eta_{s,s_1}$, and $\eta_{s,s_1} = \sqrt{[(2s_1+1)^2-s^2]/(4s^2-1)}$. We then find

$$\mathcal{H}_a|\psi_s^m\rangle = \frac{-J_a}{2}\left(G_{s,s_1}^m|\psi_s^m\rangle + \sum_{\sigma'=\pm 1}H_{s,s_1}^{m,\sigma'}|\psi_{s+2\sigma'}^m\rangle\right) \quad (6)$$

$$\mathcal{H}_c|\psi_s^m\rangle = \frac{-J_c}{8}\sum_{\sigma=\pm 1}\left(\xi_{s,s_1}F_s^{\sigma m}|\psi_s^{m+2\sigma}\rangle - \sum_{\sigma'=\pm 1}K_{s,s_1}^{\sigma m,\sigma'}|\psi_{s+2\sigma'}^{m+2\sigma}\rangle\right), \quad (7)$$

$$G_{s,s_1}^m = m^2 + (D_{s,s_1}^m)^2 + (D_{s+1,s_1}^m)^2, \quad (8)$$

$$H_{s,s_1}^{m,\sigma'} = D_{s+(\sigma'+1)/2,s_1}^m D_{s+(\sigma'+3)/2,s_1}^m, \quad (9)$$

$$\xi_{s,s_1} = \frac{2[4s_1(s_1+1)+s(s+1)]}{(2s-1)(2s+3)}, \quad (10)$$

and

$$K_{s,s_1}^{x,\sigma'} = C_{s+(\sigma'+1)/2,s_1}^{x-1}C_{s+(\sigma'+3)/2,s_1}^{x-2}. \quad (11)$$

Equations (4-5) allow for an exact solution to the most general Hamiltonian of arbitrary order in the individual spin operators. The operations of \mathcal{H}_0 , \mathcal{H}_b and \mathcal{H}_d satisfy the selection rules $\Delta s = 0$, $\Delta m = 0, \pm 1, \pm 2$. The local anisotropy interactions \mathcal{H}_a and \mathcal{H}_c allow transitions satisfying $\Delta s = 0, \pm 2$, $\Delta m = 0$ and $\Delta s = 0, \pm 2$, $\Delta m = \pm 2$, respectively, so s is no longer a good quantum number.

In order to obtain the thermodynamic properties, we first calculate the canonical partition function, $Z = \text{Tr} \exp(-\beta \mathcal{H})$. Since \mathcal{H} is not diagonal in the (s, m) representation, we must construct the wave function from all possible spin states. We then write

$$Z = \text{Tr} \langle \Psi_{s_1} | e^{-\beta \mathcal{H}} | \Psi_{s_1} \rangle, \quad (12)$$

$$\langle \Psi_{s_1} | = \prod_{s=0}^{2s_1} \prod_{m=-s}^s \langle \psi_s^m | = \langle \psi_0^0 | \otimes \langle \psi_1^{-1} | \otimes \langle \psi_1^0 | \otimes \cdots \otimes \langle \psi_{2s_1}^{2s_1} |, \quad (13)$$

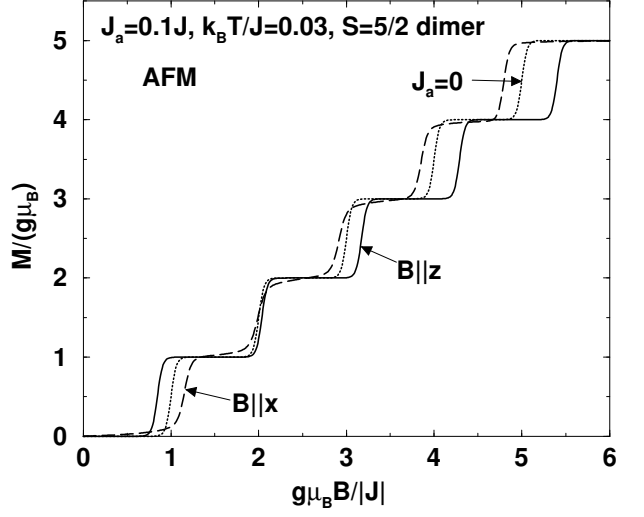


FIG. 2: Plot at $k_B T/|J| = 0.03$ and $J_a/J = 0.1$ of $M/(g\mu_B)$ versus $g\mu_B B/|J|$ for the AFM spin $5/2$ dimer. Curves for $\mathbf{B} \parallel \hat{z}$ (solid), $\mathbf{B} \parallel \hat{x}$ (dashed), and the isotropic case ($J_a = 0$, dotted) are shown.

where $\beta = 1/(k_B T)$ and k_B is Boltzmann's constant. To evaluate the trace, it is useful to diagonalize the $\langle \Psi_{s_1} | \mathcal{H} | \Psi_{s_1} \rangle$ matrix. To do so, we let $|\Psi_{s_1}\rangle = \mathbf{U}|\Phi_{s_1}\rangle$, where $|\Phi_{s_1}\rangle = \prod_{n=1}^{n_{s_1}} |\phi_n\rangle$ is constructed from the new orthonormal basis $\{|\phi_n\rangle\}$, and \mathbf{U} is a unitary matrix of rank $n_{s_1} = (2s_1 + 1)^2$. Choosing \mathbf{U} to diagonalize \mathcal{H} , we generally obtain $\mathcal{H}|\phi_n\rangle = \epsilon_n|\phi_n\rangle$ and the partition function for a SMM dimer,

$$Z = \sum_{n=1}^{n_{s_1}} \exp(-\beta \epsilon_n). \quad (14)$$

The specific heat $C_V = k_B \beta^2 \partial^2 \ln Z / \partial \beta^2$ is then easily found at all T, \mathbf{B} . The magnetization

$$\mathbf{M} = \frac{1}{Z} \sum_{n=1}^{n_{s_1}} \nabla_{\mathbf{B}}(\epsilon_n) \exp(-\beta \epsilon_n), \quad (15)$$

requires $\nabla_{\mathbf{B}}(\epsilon_n)$ for each \mathbf{B} .

Examples of C_V and of \mathbf{M} versus $|B/J|$ were given previously for the isotropic dimer.[11] Since it is easier to measure $\mathbf{M}(\mathbf{B})$ at fixed T , we focus upon it. Additional results will be published elsewhere.[20]

In Figs. 2-5, we plot $\mathbf{M}/(g\mu_B)$ versus $g\mu_B B/|J|$ for four low- T cases of AFM $s_1 = 5/2$ dimers, taking $k_B T/|J| = 0.03$, and in Fig. 6, examples of $\mathbf{M}(\theta)$ at fixed B and $\phi = 0$ are shown. In Figs. 2-6, we set $J_j/J = 0.1$ for $j = a, b, c, d$, respectively, and the other $J_j = 0$. Figures 2-6 are sufficient to illustrate the new physics that arise from the local spin anisotropy exchange interactions. In Figs. 2-5, the solid and dashed curves represent the cases of $\mathbf{B} \parallel \hat{z}$ and $\mathbf{B} \parallel \hat{x}$, and the dotted curve is the isotropic case, $J_j = 0 \forall j$. \mathcal{H}_a and \mathcal{H}_b are

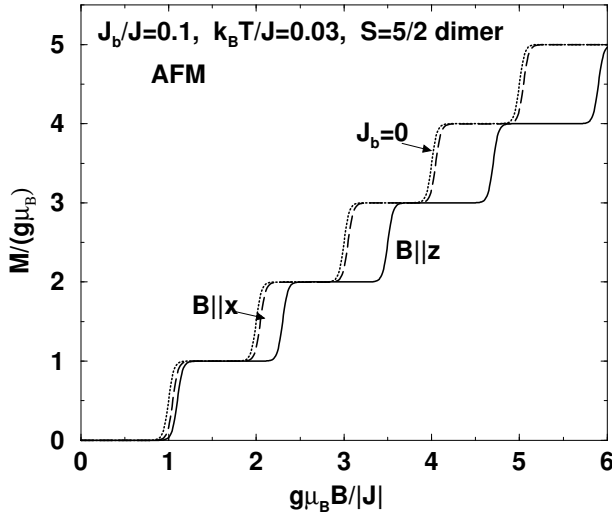


FIG. 3: Plot of $M/(g\mu_B)$ versus $g\mu_B B/|J|$ for $J_b/J = 0.1$. The other parameters and labels are as in Fig. 2.

invariant under $x \leftrightarrow y$, so curves for $\mathbf{B} \parallel \hat{x}$ in Figs. 2 and 3 are identical to those for $\mathbf{B} \parallel \hat{y}$. Since \mathcal{H}_c and \mathcal{H}_d are odd under $x \leftrightarrow y$, the $\mathbf{B} \parallel \hat{x}$ curves in Figs. 4 and 5 correspond to $\mathbf{B} \parallel \hat{y}$ with $J_c/J, J_d/J = -0.1$, respectively.

We first examine the global spin anisotropy effects of \mathcal{H}_b and \mathcal{H}_d in Figs. 3 and 5, respectively. In Fig. 3, the dotted (isotropic) curve exhibits $2s_1 = 5$ steps that are both equally high and wide as $T \rightarrow 0$. For $J_b = 0.1J$, setting $\mathbf{B} \parallel \hat{x}$ causes only a small increase in the field required for each step that is nearly independent of the step number, but a much larger, monotonic increase with step number in the field required for each step effect is obtained when $\mathbf{B} \parallel \hat{z}$. In Fig. 5, the opposite occurs. The curve for $J_d/J = 0.1$ and $\mathbf{B} \parallel \hat{z}$, normal to the anisotropy plane, is indistinguishable from the isotropic (dotted) case. However, for $\mathbf{B} \parallel \hat{x}$, there is a monotonic increase in the field required for the step with step number.

In contrast, the local field anisotropy interactions show very different behaviors. In Fig. 2, our results for the effects of the local axial anisotropy interaction \mathcal{H}_a , Eq. (1), are shown. In this case, the field anisotropy effects change sign. For $\mathbf{B} \parallel \hat{z}$ the first step appears at a lower value of $|\mathbf{B}|$ than in the isotropic case, and for steps 3-5, there is a monotonic increase in the extra field required for each step. The opposite is true for $\mathbf{B} \parallel \hat{x}$, for which the first step appears at a larger $|\mathbf{B}|$ value than for the isotropic case, and subsequent steps appear at monotonically decreasing values of $|\mathbf{B}|$. A cross-over occurs at about the second step, for which the effects of this type of anisotropy are small. These local axial anisotropy effects are very different than the global anisotropy ones pictured in Figs. 3 and 5.

In Fig. 4, we present our \mathbf{M} results for the case of local azimuthal anisotropy, \mathcal{H}_c , Eq. (2). For $\mathbf{B} \parallel \hat{z}$, there is almost no effect, as for the case of global azimuthal

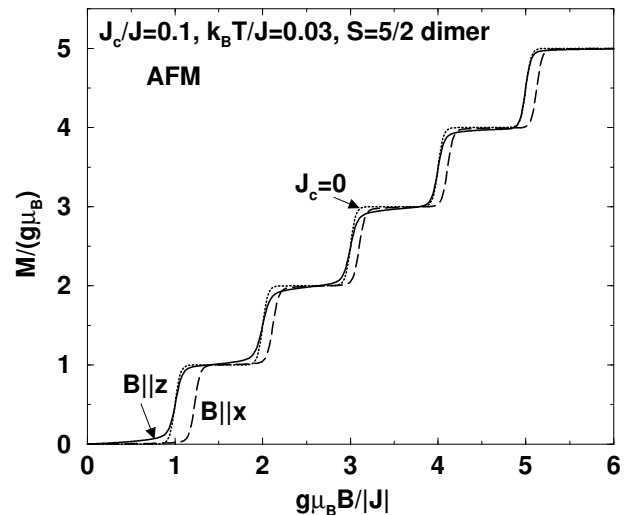


FIG. 4: Plot of $M/(g\mu_B)$ versus $g\mu_B B/|J|$ for $J_c/J = 0.1$. The other parameters and labels are as in Fig. 2.

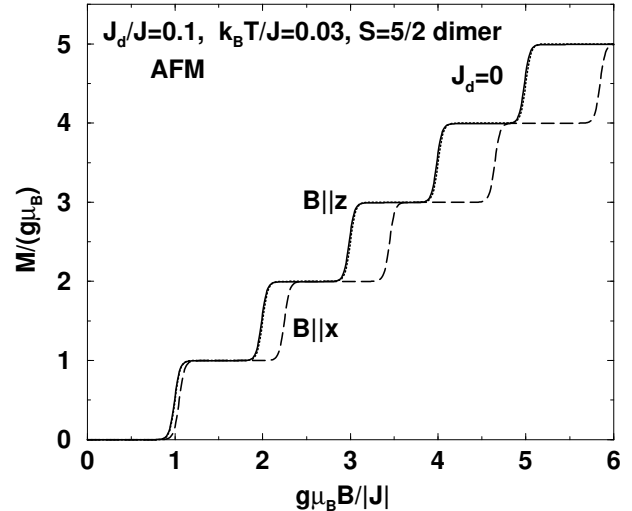


FIG. 5: Plot of $M/(g\mu_B)$ versus $g\mu_B B/|J|$ for $J_d/J = 0.1$. The other parameters and labels are as in Fig. 2.

anisotropy pictured in Fig. 5. For $\mathbf{B} \parallel \hat{x}$, the field required for each step is larger than in the isotropic interaction case, as for global azimuthal anisotropy shown in Fig. 5. However, in this local azimuthal anisotropy case, the extra field required for each step is non-monotonic in the step number, with the largest extra field required for the first step, and the minimum extra field required for the intermediate, third step. This is in stark contrast to the monotonic global anisotropy behavior.

In addition, the angular dependencies of \mathbf{M} are different for each of the four J_j . In Fig. 6, we present the results for $|\mathbf{M}(B, \theta, \phi = 0)|/(g\mu_B)$ versus θ/π near the second step at $g\mu_B|\mathbf{B}/|J| = 2.0, 2.1$ and $k_B T/|J| = 0.03$ for each of the four AFM cases pictured in Figs. 2-5. Note that $|\mathbf{M}|(B, \pi - \theta, 0) = |\mathbf{M}(B, \theta, 0)|$. The J_a and J_b

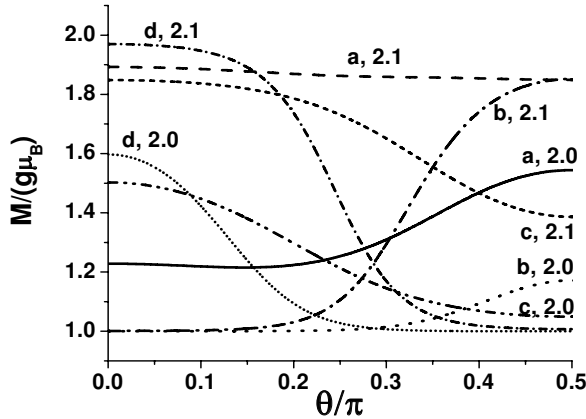


FIG. 6: Plot of $|M|(g\mu_B)$ at $\phi = 0$ versus θ/π near the second step at $g\mu_B B/|J| = 2.0, 2.1$ and $k_B T/|J| = 0.03$ for each $J_j/J = 0.1$. Curves are labelled with $j, g\mu_B B/|J|$ values.

curves, while rather similar at $g\mu_B |\mathbf{B}/J| = 2.0$, are very different at $g\mu_B |\mathbf{B}/J| = 2.1$. Hence, $\mathbf{M}(\mathbf{B})$ depends strongly upon the particular type of spin anisotropy.

We note that $s_1 = 1/2$ dimers behave very differently from higher spin dimers. For $s_1 = 1/2$, local and global spin anisotropy effects are indistinguishable, as J_a merely shifts the ground state energy, and J_c simply renormalizes J_d to $J_d + J_c/2$. In contrast, for $s_1 \geq 1$, all four of the J_j enter the Hamiltonian matrix separately. Not only are the diagonal elements containing J_a different, there are generally $2s_1$ distinct off-diagonal linear combinations of J_d and J_c , and the number of different off-diagonal elements separately proportional to either J_a or J_c increases non-linearly with s_1 . Hence, for $s_1 \geq 1$, local and global spin anisotropy effects are qualitatively different.

There were two low- T $M(B)$ studies of Fe_2 dimers.[13, 14] For μ -oxalatotetrakis(acetylacetonato) Fe_2 , all five peaks in dM/dH were measured in pulsed magnetic fields H . These evenly spaced peaks indicated little, if any, spin anisotropy effects.[13] On the other hand, studies of the first 2-3 dM/dH peaks in powdered samples of $[\text{Fe}(\text{salen})\text{Cl}]_2$, where salen is N, N' -ethylenebis(salicylideneiminato), were much more interesting.[14] These data showed a broad first peak at $B = 17 - 20\text{T}$ that was only partially resolvable into two separate peaks, followed by a sharp second peak at $B = 36\text{ T}$, consistent with local axial anisotropy of strength $|J_a/J| \approx 0.1$, as in Fig. 2, perhaps combined with a smaller $|J_c/J|$, but are inconsistent with either global anisotropy interactions pictured in Figs. 3 and 5. It appears that the interaction of a Cl^- ion neighboring each Fe^{3+} ion leads to strong local anisotropy effects. In order to verify this hypothesis and to elucidate the details of the interactions, further experiments using

single crystals in different field orientations on this and related Fe_2 dimers with 1-3 similarly bonded Cl^- ions is urged.[16, 17]

In summary, we have solved for the case of equal spin single molecule magnet dimers including the most general forms of anisotropic spin exchange interactions quadratic in the spin operators. Local anisotropy interactions lead to low- T $M(B)$ step widths that have a much richer variation with \mathbf{B} than do the global anisotropy interactions. With local anisotropy interactions, the total spin s is not a good quantum number, modifying our understanding of quantum tunneling processes. It might also be possible to fit a variety of experimental results using a smaller, consistent set of model parameters.[6] We emphasize that the study of SMM dimers, for which the most general anisotropic quadratic exchange interactions can be solved exactly, may be our best hope for attaining a more fundamental understanding of the underlying physics of single molecule magnets.

We thank the Max-Planck-Institut für Physik komplexer Systeme, Dresden, Germany and the University of North Dakota, Grand Forks, ND, USA for their kind hospitality and support. This work was supported by the Netherlands Foundation for the Fundamental Research of Matter and by the NSF under contract NER-0304665.

* Electronic address: efremov@theory.phy.tu-dresden.de

† Electronic address: klemm@phys.ksu.edu

- [1] R. Sessoli *et al.*, Nature (London) **365**, 141 (1993).
- [2] J. R. Friedman *et al.*, Phys. Rev. Lett. **76**, 3830 (1996).
- [3] M. N. Leuenberger and D. Loss, Nature (London) **410**, 789 (2001).
- [4] W. Wernsdorfer *et al.*, Phys. Rev. Lett. **82**, 3903 (1999).
- [5] W. Wernsdorfer and R. Sessoli, Science **284**, 133 (1999).
- [6] D. Zipse *et al.*, Phys. Rev. B **68**, 184408 (2003).
- [7] M. Affronte *et al.*, Phys. Rev. Lett. **88**, 167201 (2002).
- [8] O. Waldmann *et al.*, Inorg. Chem. **1999**, (38), 5879.
- [9] O. Waldmann *et al.*, Inorg. Chem. **2001**, (40), 2986.
- [10] H. Nakano and S. Miyashita, J. Phys. Chem. Solids **63**, 1519 (2002).
- [11] D. V. Efremov and R. A. Klemm, Phys. Rev. B **66**, 174427 (2002).
- [12] F. Le Gall *et al.*, Inorg. Chim. Acta **262**, 123 (1997).
- [13] Y. Shapira *et al.*, Phys. Rev. B **63**, 094422 (2001).
- [14] Y. Shapira *et al.*, Phys. Rev. B **59**, 1046 (1999).
- [15] K. L. Taft *et al.*, J. Am. Chem. Soc. **116**, 823 (1994).
- [16] J. D. Walker and R. Poli, Inorg. Chem. **1990** (29), 756.
- [17] J. A. Bertrand, J. L. Breece, and P. G. Eller, Inorg. Chem. **13**, 125 (1974).
- [18] R. Tiron *et al.*, Phys. Rev. Lett. **91**, 227203 (2003).
- [19] J. M. North *et al.*, Phys. Rev. B **69**, 174419 (2004).
- [20] D. V. Efremov and R. A. Klemm, unpublished.